New Journal of Physics
The open access journal at the forefront of physics

Deutsche Physikalische Gesellschaft DPG
IOP Institute of Physics

Published in partnership with: Deutsche Physikalische Gesellschaft and the Institute of Physics

OPEN ACCESS

RECEIVED
20 November 2015

ACCEPTED FOR PUBLICATION
25 January 2016

PUBLISHED
17 February 2016

PAPER

Caustic structures in x-ray Compton scattering off electrons driven by a short intense laser pulse

D Seipt[1,2], **A Surzhykov**[1], **S Fritzsche**[1,2] **and B Kämpfer**[3,4]

[1] Helmholtz-Institut Jena, Fröbelstieg 3, D-07743 Jena, Germany
[2] Friedrich Schiller Universität Jena, Theoretisch Physikalisches Institut, D-07743 Jena, Germany
[3] Helmholtz-Zentrum Dresden-Rossendorf, Institute of Radiation Physics, PO Box 510119, D-01314 Dresden, Germany
[4] TU Dresden, Institut für Theoretische Physik, D-01062 Dresden, Germany

E-mail: d.seipt@gsi.de

Keywords: XFEL, caustics, intense laser pulses, laser-assisted Compton scattering, strong-field QED

Abstract

We study the Compton scattering of x-rays off electrons that are driven by a relativistically intense short optical laser pulse. The frequency spectrum of the laser-assisted Compton radiation shows a broad plateau in the vicinity of the laser-free Compton line due to a nonlinear mixing between x-ray and laser photons. Special emphasis is placed on how the shape of the short assisting laser pulse affects the spectrum of the scattered x-rays. In particular, we observe sharp peak structures in the plateau region, whose number and locations are highly sensitive to the laser pulse shape. These structures are interpreted as spectral caustics by using a semiclassical analysis of the laser-assisted QED matrix element, relating the caustic peak locations to the laser-driven electron motion.

1. Introduction

X-ray free electron lasers (XFELs) help explore matter on ultra-short time-scales and under extreme conditions. Their high x-ray photon flux and short pulse duration of only a few femtoseconds allow to record transient processes like chemical reactions in real-time [1, 2]. Moreover, the x-ray scattering off dense plasmas—for instance those plasmas generated by irradiating a solid density target with an ultra-intense optical laser pulse [3]—facilitate the study of ultra-fast collective dynamics and plasma instabilities [4–7], which are important for novel particle acceleration [8–10] or fusion energy concepts [3], for instance.

Such extreme states of matter can be generated with the help of optical lasers that reached already intensities of 10^{22} W cm^{-2} [11]. The interaction of such laser pulses with electrons (with charge e and mass m) is characterised by the laser's normalised amplitude $a_0 = |e|E_\mathrm{L}/m\omega_\mathrm{L}$, where ω_L and E_L are the frequency and amplitude of the laser electric field, respectively. Already for 10^{18} W cm^{-2} ($a_0 \sim 1$), the electron's quiver motion reaches relativistic velocities and its interaction with the laser's magnetic field leads to a nonlinear orbital motion, often denoted as 'figure 8' [12]. At extreme light intensities, $a_0 \gg 1$, the electrons interact with many photons from the laser field simultaneously and one enters the realm of non-perturbative strong-field quantum electrodynamics (QED) [13–15].

High-intensity lasers can also be employed in laser-assisted scattering processes [16–32], where the presence of the strong low-frequency laser field modulates a hard QED scattering process. This could be, for instance, Compton scattering where a hard x-ray (or γ-ray) photon is scattered off a (quasi-)free electron with a frequency change that depends on the scattering angle [33]. The assisting strong low-frequency laser field leads to the formation of side-bands in the frequency spectrum close to the laser-free Compton line due to x-ray—optical frequency mixing. Already for $a_0 \sim 1$ the electron interacts with a large number of laser photons [34].

In this paper, we present a QED description of laser assisted Compton scattering [34–39] of an ultra-short pulse of coherent x-rays from an XFEL off electrons moving in an intense ($a_0 \sim 1$) and ultra-short synchronised optical laser pulse [40–42]. In contrast to previous works we analyse for the first time in detail the structures in the frequency spectrum of the scattered x-rays with regard to the influence of the specific shape and duration of

the assisting laser pulse, and how these structures are related to the ultra-fast laser-driven electron motion. By developing a semiclassical picture we identify the prominent peaks in the spectrum as *spectral caustics* emerging from coalescing stationary phase points where the quantum scattering amplitude is formed.

Caustics are a phenomenon known best from wave propagation. They occur when the rays associated to a wave field coalesce on a manifold of lower dimension, creating bright zones in the wave field. A well known example is the focal spot of a lens: all parallel light rays that impinge on the lens coalesce in a single point—the focal point. From the mathematical viewpoint, caustics are singularities of differentiable mappings [43, 44] and also occur in the spectral domain [45]. The notion of spectral caustics enables us to explain why the plateau region in the frequency spectrum is not flat, but has peaks at certain frequencies.

Our paper is organised as follows: in section 2 we describe the physical system, and lay out the basic theory, providing an expression for the QED cross section. Moreover, numerical results are provided for the complex frequency spectra of the scattered x-rays. From a semiclassical analysis of the scattering dynamics in section 3 we conclude that the peaks in the frequency spectrum can be interpreted as spectral caustics, and we calculate the caustic peak locations. In section 4 we discuss a possible scenario for the experimental observation of the spectral caustic peaks, taking into account various non-ideal effects. We summarise and conclude in section 5. In two appendices we give a brief derivation of the cross section (appendix A) and we present a method to efficiently calculate frequency-averaged spectra (appendix B).

2. Theoretical description: the QED cross section

In our theoretical modelling of laser-assisted Compton scattering we describe the incident light of the XFEL (X) and assisting laser (L) as pulsed plane waves with frequencies $\omega_{\mathrm{X,L}}$ and durations $T_{\mathrm{X,L}}$. They copropagate along the z-direction, described by the unit four-vector $n^\mu = (1,\,0,\,0,\,1)$, with mutually orthogonal linear polarisation four-vectors $\varepsilon^\mu_{\mathrm{X,L}}$. That means the laser photon four-momentum is given by $k^\mu_{\mathrm{L}} = \omega_{\mathrm{L}} n^\mu$ and $k^\mu_{\mathrm{X}} = \omega_{\mathrm{X}} n^\mu$ for the x-rays accordingly. These light pulses scatter off a free electron that has the four-momentum p^μ prior to the interaction. We assume the x-rays to be a *weak field* in the sense that just one x-ray photon interacts with the electron in a single scattering event [34]. The scattered x-ray photon has four-momentum $k'^\mu = \omega' n'^\mu$, with frequency ω' and scattering direction $n'^\mu = (1,\,\sin\vartheta\cos\varphi,\,\sin\vartheta\sin\varphi,\,\cos\vartheta)$, where ϑ is the scattering angle, measured from the initial laser beam direction, and φ denotes the azimuthal angle relative to the laser polarisation direction. We employ units with $\hbar = c = 1$ and the fine structure constant $\alpha = e^2/4\pi$. Scalar products between four-vectors are denoted as $x\cdot p = x^0p^0 - \boldsymbol{xp}$.

In order to calculate the cross section for laser-assisted Compton scattering in an intense laser pulse with $a_0 \gtrsim 1$ it is necessary to treat the interaction of the electrons with the assisting laser non-perturbatively. This can be achieved by working in the Furry picture, where the electron dynamics in the laser field is described by means of Volkov states [46] and the emission of photons by these laser-dressed electrons is treated in perturbation theory [13, 47]. The frequency- and angle-differential cross section for laser-assisted Compton scattering can be expressed as

$$\frac{\mathrm{d}^2\sigma}{\mathrm{d}\omega'\mathrm{d}\Omega} = \frac{\alpha^2\omega'}{8\pi m^2\int_{-\infty}^{\infty}\mathrm{d}\phi\; g_{\mathrm{X}}^2(\phi)}\frac{\langle|\mathcal{M}|^2\rangle}{(k_{\mathrm{L}}\cdot p)(k_{\mathrm{L}}\cdot p - k_{\mathrm{L}}\cdot k')}, \tag{1}$$

where g_{X} denotes the temporal envelope of the x-ray pulse, $\phi = \omega_{\mathrm{L}}(t-z)$ is the laser phase, and $\mathcal{M}$ refers to the scattering amplitude. For unpolarised electrons and unobserved polarisation of the scattered x-rays, the squared scattering amplitude can be conveniently represented as a double-integral over the laser phase ϕ

$$\langle|\mathcal{M}|^2\rangle = 2\,m^2\int\mathrm{d}\phi\mathrm{d}\phi'\; g_{\mathrm{X}}(\phi)g_{\mathrm{X}}(\phi')\mathrm{e}^{\mathrm{i}\int_{\phi'}^{\phi}\mathrm{d}\phi''\;\psi(\phi'',\ell)}\left(\eta - 2\alpha_{\mathrm{X}}^2 - \frac{\alpha_{\mathrm{X}}^2}{2}\eta\,[a_{\mathrm{L}}(\phi) - a_{\mathrm{L}}(\phi')]^2\right). \tag{2}$$

Some details of the derivation of equations (1) and (2) are provided in appendix A. Here, $a_{\mathrm{L}}(\phi)$ denotes the laser's normalised vector potential and we abbreviate

$$\eta = 2 + \frac{x^2}{1+x}, \tag{3a}$$

$$x = \frac{n\cdot k'}{n\cdot p - n\cdot k'}, \tag{3b}$$

$$\alpha_{\mathrm{X}} = \frac{mx}{\omega_{\mathrm{X}}}\left(\frac{\varepsilon_{\mathrm{X}}\cdot p}{n\cdot p} - \frac{\varepsilon_{\mathrm{X}}\cdot k'}{n\cdot k'}\right). \tag{3c}$$

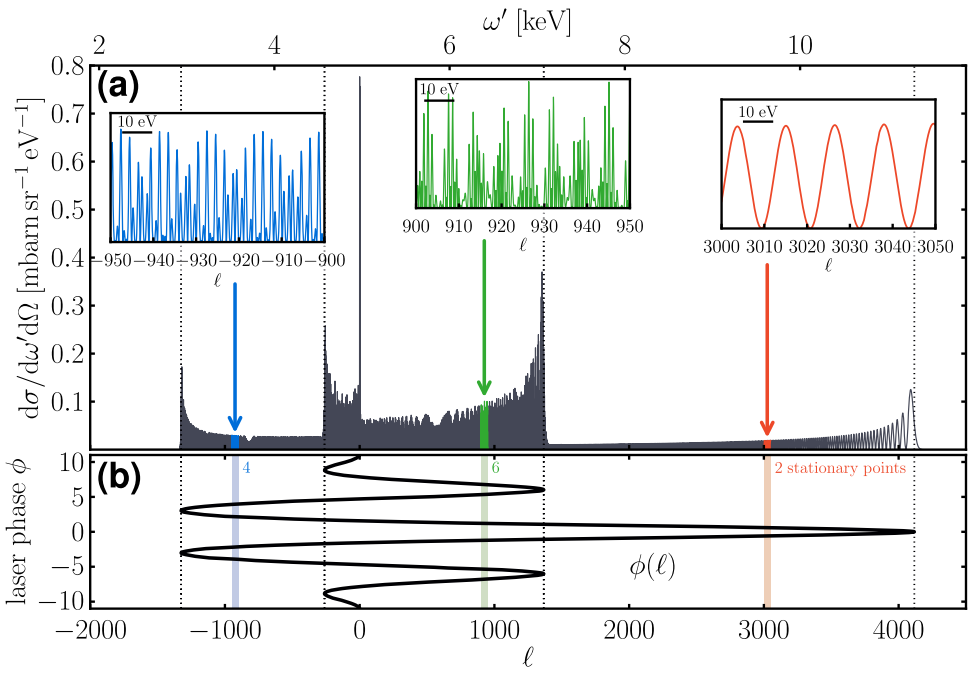

Figure 1. Frequency spectrum of x-rays that are Compton scattered off laser-driven electrons (a) as a function of the scattered x-rays' frequency ω' (upper axis) and the energy transfer ℓ (lower axis). The initial x-ray pulse has a frequency of $\omega_X = 5$ keV and a duration of $T_X = 7$ fs. The assisting laser field that drives the electron-motion has peak amplitude $a_0 = 1$, frequency ω_L=1.55 eV and pulse duration $T_L = 5$ fs. The insets magnify the highly oscillatory structure of the spectrum for three frequency ranges. Panel (b) depicts the function $\phi(\ell)$ from inverting (7), which determines the number and positions of the stationary points for a given value of ℓ. Spectral caustics appear at those ℓ where the function $\phi(\ell)$ has vertical tangents and two stationary points coalesce (vertical dotted lines).

The phase of the scattering amplitude (2) is determined by

$$\psi(\phi, \ell) = (\ell + \varkappa)\frac{n' \cdot v_L(\phi)}{n' \cdot v_0} - \varkappa, \tag{4}$$

where $\varkappa = \omega_X/\omega_L$ denotes the ratio of the x-ray and assisting laser frequencies.

The Lorentz invariant quantity ℓ describes the energy transfer from the laser field to the scattered x-ray photon and determines its frequency ω' via the nonlinear x-ray—optical frequency mixing [34, 48]:

$$\omega'(\ell) = \frac{(\omega_X + \ell\omega_L)n \cdot p}{p \cdot n' + (\omega_X + \ell\omega_L)n \cdot n'}. \tag{5}$$

The effective range of ℓ, and hence also ω', can be quite large even for $a_0 < 1$, reaching values of $\ell \sim a_0\varkappa$ for large frequency ratios $\varkappa$ [34].

Expression (4) that determines the phase of the scattering amplitude depends on the four-velocity of a classical electron moving in the laser field $a_L^\mu(\phi)$

$$v_L^\mu(\phi) = v_0^\mu - a_L^\mu(\phi) + n^\mu\frac{a_L(\phi) \cdot v_0}{n \cdot v_0} - n^\mu\frac{a_L^2(\phi)}{2n \cdot v_0}, \tag{6}$$

where $v_0^\mu = p^\mu/m$ is the electron's four-velocity before the laser pulse arrives. In equation (6), the terms linear in a_L describe the electron's quiver motion due to the laser electric field with frequency ω_L. The a_L^2-term describes the interaction with the magnetic field and comprises both a longitudinal $2\omega_L$ oscillation and a ponderomotive drift [12, 49, 50]. The superposition of the ω_L and $2\omega_L$ oscillations is often denoted as 'figure 8' motion.

Figure 1 (a) displays the frequency spectrum of Compton scattered x-rays, equation (1), for a scattering angle of $\vartheta = 45°$ in the plane of the laser polarisation, $\varphi = 0$. For convenience, from now on we work in the rest frame of the initial electron, where $v_0^\mu = (1, 0, 0, 0)$. We find a narrow large peak of laser-free Compton scattering at $\ell = 0$, which stems from x-ray photons that scatter outside the assisting laser pulse and, hence, with no energy exchanged between the electron and the laser field. Due to the action of the laser field and the frequency mixing (5) the spectrum has a broad structured plateau region between 3 and 11 keV with a number prominent large peak structures that we identify below as spectral caustics. In the regions between the caustics the spectrum is a highly oscillating function of ω' on the scale of sub-eV, as can be seen in the insets of figure 1 (a).

3. Semiclassical interpretation of the spectral peaks as spectral caustics

To gain an intuitive understanding for the complex peak structure in the spectrum in figure 1 and their relation to the laser-driven electron motion, equation (6), it is useful to put forth a semiclassical trajectory picture by applying a stationary phase analysis [26, 51, 52]. For *laser-induced* strong-field QED processes, discussed e.g. [26, 52], such a semiclassical picture is valid only for $a_0 \gg 1$. Here, for the *laser-assisted* Compton scattering process the condition $\varkappa a_0 \gg 1$ is sufficient. That means a semiclassical trajectory picture becomes reliable already for $a_0 \sim 1$ for a large ratio of the frequency scales of the hard QED process and the assisting laser field $\varkappa = \omega_X/\omega_L \gg 1$. Since the integrand of (2) is a highly oscillating function of the laser phase ϕ for $a_0\varkappa \gg 1$, the scattering amplitude, equation (2), is formed mainly at those laser phases that fulfil the stationarity condition $\psi(\phi, \ell) = 0$. Solving this implicit equation maps the scattering of x-ray photons at a certain moment ϕ to one particular value of the energy transfer

$$\ell(\phi) = \varkappa\left(\frac{n'\cdot v_0}{n'\cdot v_L(\phi)} - 1\right) \tag{7}$$

and, by means of equation (5), to one unique frequency $\omega'(\phi)$. The semiclassical analysis of the laser-assisted Compton scattering process facilitates the following interpretation: the laser-driven electron moves classically according to equation (6), up to the laser phase ϕ, where the x-ray photon scatters off the electron. At the moment of scattering the electron has acquired the velocity $v_L^\mu(\phi)$ due to its interaction with the assisting laser field. Because the x-ray photon now scatters off a relativistic electron, its frequency is Doppler shifted [33], and the Doppler shift

$$\mathfrak{D}(\phi) = \frac{n\cdot v_0}{n'\cdot v_L(\phi)} \tag{8}$$

depends on the angle between the scattering direction n' and the instantaneous electron four-velocity $v_L^\mu(\phi)$ at the moment of scattering. The Doppler factor becomes maximal when the photon is scattered in the direction of the instantaneous electron three-velocity $\boldsymbol{v}_L(\phi)$. Then, the four-vector product $n'\cdot v_L(\phi)$ is as small as possible since the three-vectors $\boldsymbol{n}'$ and $\boldsymbol{v}_L(\phi)$ are parallel. With the help of $\mathfrak{D}(\phi)$, the instantaneous frequency of the scattered x-rays can be written as

$$\omega'(\phi) = \frac{\mathfrak{D}(\phi)\omega_X}{1 + \frac{n\cdot n'}{n\cdot p}\mathfrak{D}(\phi)\omega_X}. \tag{9}$$

Thus, in the semiclassical picture the broad plateau in the frequency spectrum in figure 1 is formed because the x-ray photons scatter off accelerated electrons with a variable Doppler factor. Moreover, the frequency red-shift due to the electron recoil—the second term in the denominator of equation (9)—depends also on the instant of scattering.

The structures observed in the plateau-region of the spectrum in figure 1 can be explained by elaborating further the semiclassical picture of the laser-assisted QED scattering process. The semiclassical mapping (7), relates a moment of scattering ϕ to a *unique energy transfer* $\ell(\phi)$. However, as seen from figure 1 (b), the inverse function $\phi(\ell)$ is multiple-valued. Thus, the probability to observe a scattered x-ray photon with a particular frequency $\omega'(\ell)$ is determined by multiple stationary points. The contributions to the squared scattering amplitude from different stationary phase points interfere and that leads to the highly oscillatory behaviour of the frequency spectrum in figure 1. For instance, in the region around $\ell \approx 3000$ two stationary points contribute to the scattering amplitude, leading to a cosine-like oscillation of the spectrum (right inset), while around $\ell \approx 900$ (middle inset) a total of six stationary points are relevant providing a more complex structure with multiple oscillation periods.

We now come to an interpretation of the large sharp peaks in the plateau region of the frequency spectrum. These peaks occur at those values of ℓ, where two branches of $\phi(\ell)$ merge, i.e. two stationary points coalesce, and the function $\phi(\ell)$ has vertical tangents, see figure 1. Such singularities of the semiclassical mapping $\phi(\ell)$ are spectral caustics, specifically caustics of the fold-type A_2, i.e. locally the semiclassical mapping can be approximated by a polynomial $\phi^2 + \text{const.} = 0$ [44]. Moreover, the stationary phase approximation of the squared matrix element diverges at the caustics. By using a uniform asymptotic expansion the caustic contribution to the the spectrum can be approximated as an Airy function [44]. As caustics, the spectral peaks have some universal properties such as the their asymmetric shape, and they are characterised by universal indices. For instance, the so-called index of the caustic zone $\alpha_c = 2/3$ allows to give an order of magnitude estimate for the width of the spectral caustic peaks as $\Delta\ell \sim (a_0\varkappa)^{2/3}$, and which agrees fairly well with our numerical calculations.

However, how can one understand the existence of the spectral caustic peaks from a physical viewpoint? The divergence of $\phi(\ell)$ implies that the caustics are formed at those parts of the electron trajectory where the

Doppler factor $\mathfrak{D}(\phi_c)$ becomes stationary, $\dot{\mathfrak{D}}(\phi_c) = 0$, and the scattered x-rays have constant frequency over a long phase region. This generates a peak in the spectrum by 'focusing' the scattered radiation to the spectral caustic peak at $\omega'(\phi_c)$. The stationarity of the Doppler factor implies that at the caustic formation phase ϕ_c the four-acceleration of the electron is perpendicular to the scattering direction: $n' \cdot \dot{v}_L(\phi_c) = 0$.

Let us now calculate, within the semiclassical picture, the locations of the spectral caustic peaks in the frequency spectrum of the scattered x-rays and how they depend on the scattering direction n'. For that, we first have to solve the caustic condition $n' \cdot \dot{v}_L(\phi_c) = 0$ for the phase ϕ_c, where the caustics are formed. Employing equation (6), we can write the caustic condition as

$$0 = \dot{f}_L(\phi_c)[a_0 f_L(\phi_c) - B(\vartheta, \varphi)], \tag{10}$$

with the laser pulse shape f_L and

$$B(\vartheta, \varphi) = \frac{\cos\varphi \sin\vartheta}{\cos\vartheta - 1}. \tag{11}$$

Because equation (10) consists of the product of two terms we actually find two different classes of spectral caustics with distinct properties, which we denote as regular and irregular caustics, respectively.

The positions of the regular caustic peaks in the frequency spectrum can be determined by solving $\dot{f}_L(\phi_c) = 0$ for the caustic formation phases ϕ_c. For instance, for laser pulses $f_L = g_L \cos(\phi + \phi_0)$ with a slowly varying envelope g_L, with $\dot{g}_L/g_L \ll 1$, and the carrier envelope phase ϕ_0, the caustics are formed at the laser phases $\phi_c^{(n)} \approx n\pi - \phi_0$, $n = 0, \pm 1, \ldots$. For ultra-short pulses, with $\dot{g}_L/g_L \sim 1$, the caustic formation phases $\phi_c^{(n)}$ need to be obtained numerically. Plugging the solutions for $\phi_c^{(n)}$ into equation (7), we obtain the locations of the regular spectral caustics at

$$\ell_{\mathrm{reg}}^{(n)} = \ell(\phi_c^{(n)}) = \varkappa \frac{\xi^{(n)}}{1 - \xi^{(n)}},$$
$$\xi^{(n)} = (-1)^{n+1} a_0 g_L(\phi_c^{(n)}) \cos\varphi \sin\vartheta - \frac{a_0^2}{2} g_L^2(\phi_c^{(n)})(1 - \cos\vartheta). \tag{12}$$

They depend on the value of the laser vector potential $a_L(\phi_c^{(n)})$ at its local extrema, and, therefore, on the carrier envelope phase ϕ_0 and on the shape and duration of the pulse, see figure 2.

Let us now discuss what this tells us about the locations and the distribution of the spectral caustic peaks in the plateau region. Consider first a smooth laser pulse, e.g. with a squared cosine envelope

$$g_L(\phi) = \begin{cases} \cos^2 \dfrac{\pi\phi}{2\omega_L T_L}, & |\phi| \leqslant \omega_L T_L, \\ 0, & \text{elsewhere}, \end{cases} \tag{13}$$

with pulse duration T_L. Because the envelope smoothly increases from 0 to 1, the laser pulse envelope at the caustic formation phase $g_L(\phi_c^{(n)})$ can take any value between zero and one. Thus, the spectral caustics (12) are equally distributed over the whole plateau region of the spectrum, as can be seen well in figure 2, panels (a)–(c). The number of different spectral caustic peaks in the panels (a)–(c) grows with increasing laser pulse duration T_L because the number of local extrema of $a_L(\phi)$ increases with T_L (see insets in figure 2). In order to resolve the individual caustic peaks, their separation should be larger larger than their individual width $\Delta\ell \sim (a_0\varkappa)^{2/3}$. This gives the order of magnitude estimate of the optimal laser pulse duration as $\omega_L T_L \sim (a_0\varkappa)^{1/3}$.

The situation is quite different for a box-shaped envelope with a constant amplitude, see figure 2 (d). Only two regular caustic peaks occur at the endpoints of the plateau, and irrespective of the pulse duration. The reason for this behaviour is that $g_L(\phi_c^{(n)}) = 1$ for all caustic formation phases $\phi_c^{(n)}$. This 'wing'-like shape of the plateau is a generic feature of laser-assisted processes when the laser pulse has a constant amplitude and was also seen in laser-assisted electron-ion recombination [20]. Hence, in order to describe the peaks in the frequency spectrum correctly it is essential to exactly take into account the shape of the short laser pulse.

Let us now consider the irregular type of caustics. In contrast to the regular caustics, the irregular type is restricted to certain observation directions. (So far we were discussing only those directions where solely regular caustics exist.)The irregular caustic occurs where $f_L(\phi_c) = B(\vartheta, \varphi)/a_0$ admits at least one real solution for ϕ_c. In stark contrast to the regular caustics discussed above the location of the irregular caustic peak at

$$\ell_{\mathrm{irr}} = \varkappa \frac{\zeta}{1 - \zeta}, \qquad \zeta = \frac{1 - \cos\vartheta}{2} B^2(\vartheta, \varphi), \tag{14}$$

is independent of the laser pulse parameters. Although $f_L(\phi_c) = B(\vartheta, \varphi)/a_0$ might have more than one solution ϕ_c, there will be only a single spectral caustic peak in the frequency spectrum. If it exists, the irregular caustic peak always marks the high-energy cut-off of the frequency spectrum.

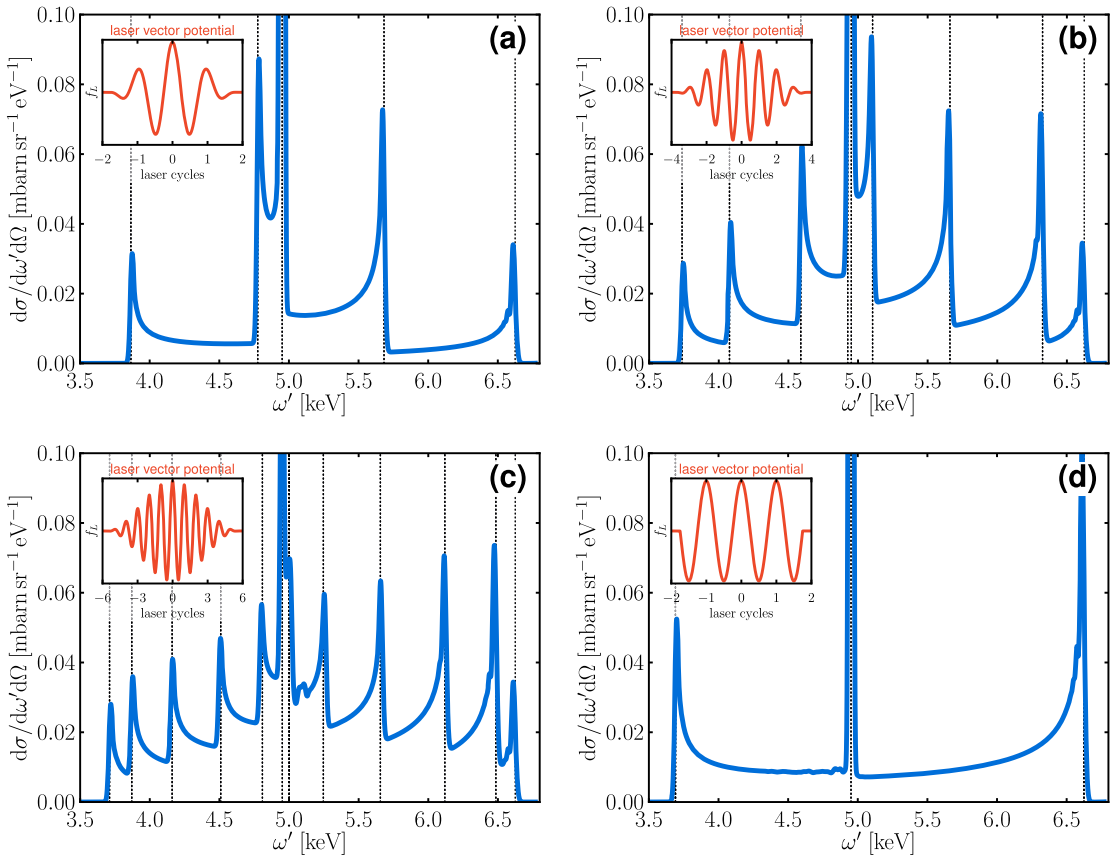

Figure 2. The number and locations of the spectral caustic peaks in frequency spectrum of the scattered x-rays depends on both the shape and duration of the driving optical laser pulse (here with peak amplitude $a_0 = 0.3$). The spectra are window-averaged (by a Gaussian with resolution 5 eV) to smooth the fast oscillations. Calculations are for a squared-cosine pulse with pulse durations $T_L = 5$ fs (a), 10 fs (b) and 15 fs (c), and for a box shaped pulse with duration 9.34 fs (d). The vertical lines depict the calculated locations of the spectral caustics. The large laser-free Compton peak at $\omega' = 4.95$ keV stems from the long x-ray pulse duration $T_X = 25$ fs $> T_L$.

The irregular caustic peak is related to the longitudinal nonlinear motion of the electrons due to the a_L^2—term in the classical electron velocity, equation (6). Therefore, it can occur only for large enough scattering angles $\vartheta \geqslant \vartheta_\star$, where one probes dominantly the longitudinal components of the electron velocity (6).

An approximate analytic expression for the angle $\vartheta_\star$ can be given as $\vartheta_\star \simeq \arccos \frac{a_0^2 - \cos^2\varphi}{a_0^2 + \cos^2\varphi}$, which gives $\vartheta_\star \simeq 67°$ for the parameters in figure 3. Exactly at the angle $\vartheta = \vartheta_\star$ a branching of the caustics occurs. Close to the branching angle $\vartheta \approx \vartheta_\star$ the semiclassical mapping (7) needs to be approximated locally by a fourth-order polynomial $\phi^4 + h(\vartheta)\phi^2 + \text{const.} = 0$, with a conveniently rescaled laser phase ϕ. The coefficient $h(\vartheta)$ is a monotonically decreasing function of ϑ, with a single zero at $\vartheta = \vartheta_\star$, where h changes its sign. Hence, for $\vartheta < \vartheta_\star$ we find only a single extremal point at $\phi = 0$, corresponding to a regular caustic. At $\vartheta > \vartheta_\star$ we find in total three extrema: the one at $\phi = 0$ remains, while two additional solutions at $\phi = \pm\sqrt{-h/2}$ give rise to the irregular caustic peak.

The Doppler up-shift of the x-ray frequency for backward-scattering (i.e. for large scattering angles) is limited by the longitudinal ponderomotive drift of the electron away from the observer. This is related to the forward–backward asymmetry seen in figure 3 (a), where high-energy photons are emitted only for $\vartheta < 90°$. Thus, the existence of the irregular caustic peak in the spectrum signals the nonlinear relativistic motion of the electrons, which comprises both the longitudinal ponderomotive drift and $2\omega_L$ oscillations. In fact, the semiclassical mapping $\ell(\phi)$, equation (7), exhibited in figures 3 (b) and (c), shows distinct $2\omega_L$—oscillations wherever the irregular caustic peak exists.

4. Discussion

Experiments on laser-assisted Compton scattering to verify the spectral caustic peaks in the spectrum could be done, e.g. at the future HIBEF beamline at the European XFEL [53] or the LCLS, where an intense optical laser beam is synchronised to the XFEL x-ray pulses. One could, for instance, scatter the x-rays off

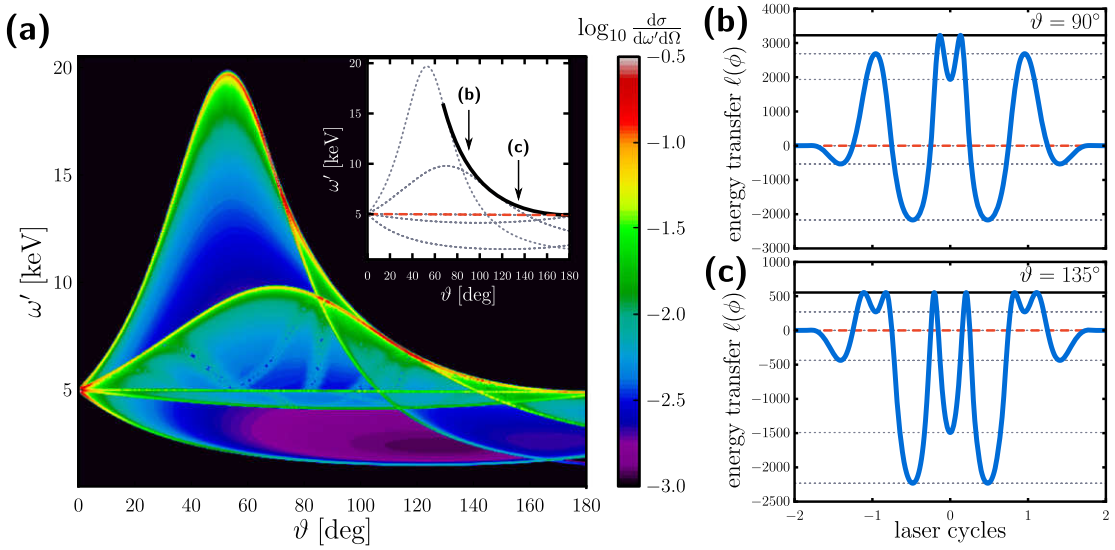

Figure 3. The frequency- and angle-differential cross section for $a_0 = 1.5$, windowed by a Gaussian of 10 eV width (a). The pattern of the sharp peaks in the spectrum qualitatively coincides with the locations of the regular (grey dotted curves) and irregular (black solid curve) spectral caustics in the inset. The red dashed curve is the laser-free Compton line. Parameters are as in figure 1. In (b) and (c) the energy transfer $\ell(\phi)$ oscillates with a frequency $2\omega_L$ close to the irregular caustics. The horizontal lines have the same meaning as in the inset of panel (a).

counterpropagating low-energy electrons with kinetic energies (of a few keV) emitted from an electron gun [54]. The principal set-up of such a scenario was discussed previously in [34], where the observation of the plateau, i.e. the x-ray—optical frequency mixing, was proposed by a using an x-ray detector with a coarse spectral resolution of $\mathcal{O}(100\text{ eV})$, characteristic for an x-ray CCD. Obviously it is impossible to resolve the individual caustic peaks, with such a coarse spectral resolution. We will return to the case of a detector with coarse resolution at the end of this section. But let us first discuss what would be required to actually see the spectral caustic peaks themselves. In order to resolve the spectral caustic structures in the plateau region of the frequency spectrum one of course needs x-ray detectors with a much better energy resolution than the ones discussed above. Microcalorimeter arrays, as an example, provide the necessary spectral resolution in a large frequency range from a few keV up to several 100 keV [55, 56]. For instance, in [56], a spectral resolution of 2 eV FWHM was reported for x-rays up to 6 keV.

In order to assess the observability of the spectral caustic peaks we need to discuss several non-ideal effects. Firstly, we need to take into consideration that each detector has a finite size and therefore covers a finite solid angle range. Since the positions of the caustics in the spectrum depend sensitively on the scattering angles $(\vartheta,\ \varphi)$ one might argue that the caustic peaks could disappear from the spectrum when a finite-sized detector collects photons in different directions. To test the viability of our results with regard to a finite detector size we integrate the frequency- and angle-differential cross section, equation (1), over the solid angle range $85° \leqslant \vartheta \leqslant 95°$ and $175° \leqslant \varphi \leqslant 185°$. In order to efficiently calculate the spectra for many different angles we employ the approximation presented in appendix B. The results of the angular integration, exhibited in figure 4 (a), shows that the spectral caustic peaks in fact do survive, despite becoming slightly broader.

As a second important issue we have to take into account the rather low total scattering cross section for x-rays on free electrons on the order of the Thomson cross section, $\sigma_T \simeq 665$ mbarn, and the low electron density in an electron beam. Therefore one most likely has to perform multi-shot experiments in order to record the complete frequency spectrum. However, it is known that present-day high-intensity lasers suffer from shot-to-shot fluctuations of, e.g., the pulse duration and peak intensity. Given the sensitive dependence of the predicted caustic peak positions on the laser pulse parameters one might again argue that those fluctuations could completely wash out all spectral peaks. This, however, is not the case. To confirm that the spectral caustic peaks survive shot-to-shot fluctuations when averaging over multiple laser shots, we calculate an ensemble of spectra for fluctuating values of a_0 and T_L, respectively, and weighted them with a Gaussian distribution with 10% FWHM, and centred around $a_0 = 0.3$, respectively $T_L = 5$ fs. The averaged spectra are exhibited in figures 4 (b) and (c) and show that the caustic peaks are still visible, despite being broadened.

The positions of the caustic peaks are insensitive with regard to the amplitude and duration of the x-ray pulse, because the laser-assisted Compton process is linear in the incident x-ray photon field. The caustic peak positions are determined solely by the strong assisting laser pulse and the relativistic electron motion it causes.

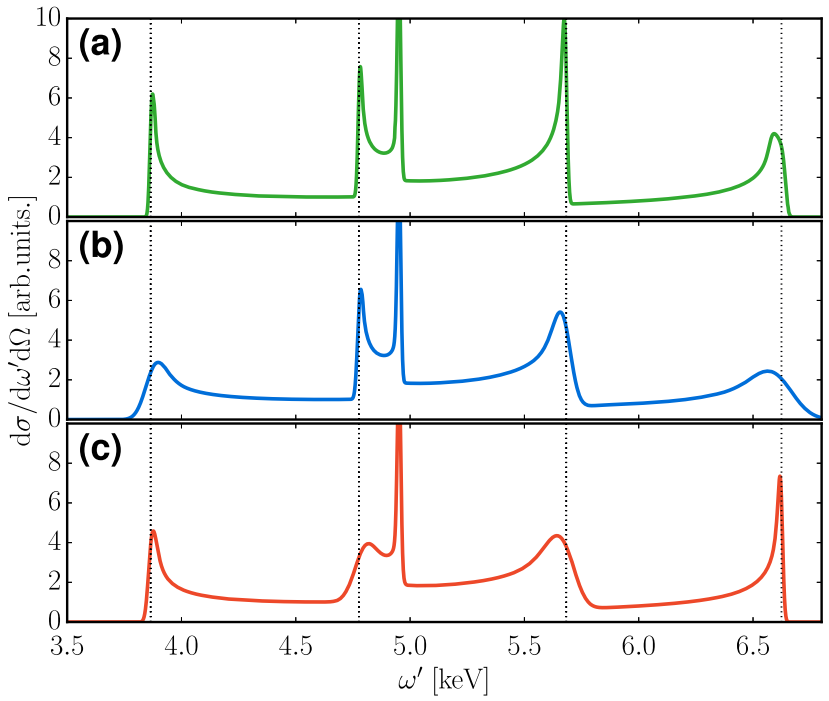

Figure 4. As figure 2 (a), but taking into account non-ideal effects, and for $T_X = 8$ fs. (a) Integration over a finite detector size. (b) Averaging over fluctuating values of a_0. (c) Averaging over fluctuating laser pulse duration T_L. For details see the text.

Since a good temporal overlap of the x-ray and assisting laser pulses is required, and taking into account the temporal jitter of both pulses, the best scenario would involve an x-ray pulse duration 2…3 times longer than the duration of the assisting laser pulse. The x-rays that are scattered outside the assisting laser pulse just contribute to the laser-free Compton line at $\ell = 0$, and do not affect the spectrum in the plateau region where the spectral caustics occur.

The actual source size of the scattered x-ray photons in the plateau region of the spectra is just the spatial volume where the two foci of the x-ray beam and the assisting laser beam overlap. Only rather moderate laser intensities of $10^{17}\ldots10^{18}$ W cm^{-2} (e.g. $a_0 = 0.3$ corresponds to 2×10^{17} W cm^{-2} at a wavelength of 800 nm) are required to observe the spectral caustic features. Such intensities can be routinely obtained by even moderately sized high-intensity lasers (a few terawatts) in quite large spot sizes of several tens of μm, and with high repetition rates. Focusing the XFEL beam to a considerably smaller size than the focal spot size of the assisting laser field, say a few μm, one can achieve a homogeneous intensity of the assisting laser field over the whole interaction region. Thus, the approximation of a constant a_0 over the interaction region (plane-wave approximation) is well justified.

We also need to take into account that in reality the initial electron cannot be at rest because it would be expelled from the high-intensity regions by ponderomotive scattering [57, 58]. However, the minimum kinetic energy of the electrons that is required to access the laser focal spot is on the order of a few keV or less [34]. For such low-energy electron beams the patterns of caustics in the laboratory frame virtually coincide even quantitatively with the spectra in the rest frame of the incident electron which we presented here. For electrons with higher energies that counterpropagate the incident light beams with four-velocity $v_0^\mu = (\gamma,\ 0,\ 0,\ -\beta\gamma)$, where γ refers to the Lorentz factor of the electron and $\beta = \sqrt{1-\gamma^{-2}}$, the spectra from the rest-frame of the electron need to be Lorentz-transformed to the laboratory frame. This concerns in particular the frequency ω' and the scattering angle ϑ of the scattered photon, which transform as

$$\omega'_{\rm lab} = \omega'\gamma(1 - \beta\cos\vartheta), \tag{15}$$

$$\cos\vartheta_{\rm lab} = \frac{\cos\vartheta - \beta}{1 - \beta\cos\vartheta}. \tag{16}$$

The azimuthal angle φ needs not to be Lorentz transformed for head-on collisions. For the scattering off high-energy electrons with $\gamma \gg 1$, the x-ray photons would be dominantly scattered into a narrow cone with aperture angle $\vartheta_{\rm lab} \sim 1/\gamma$ around the direction of the incident electron beam. Moreover, the scattered photons frequency is additionally Doppler up-shifted as is well known from inverse Compton x-ray sources [50, 59–63], see for instance equation (8), where, e.g., $n \cdot v_0 = \gamma(1 + \beta) > 1$. Therefore, the scattering off low-energy

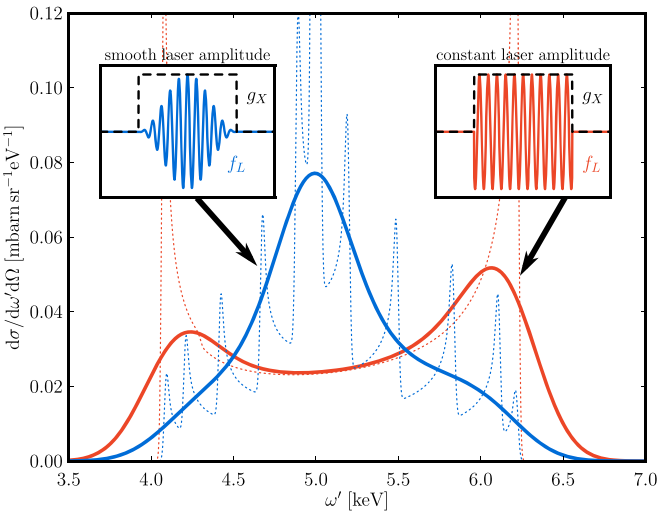

Figure 5. Coarse-grained frequency spectra. The frequency spectra have been window-averaged with 100 eV width, mimicking a detector with a coarse spectral resolution (solid curves). We compare a smooth $\cos^2$ pulse (blue) and a pulse with constant amplitude (red). Although the individual caustic peaks cannot be resolved, the shape of the plateau strongly depends on the shape of the assisting laser pulse which determines the positions of the caustic peaks in the plateau. For convenience, we exhibit by the dashed curves the spectra averaged with 10 eV detector resolution, where the distribution of the caustic peaks is still clearly visible.

electrons seems to be favourable because the scattered photons can be observed at a large scattering angle to better discriminate them from the beam of incident photons.

Because the X and L beams are parallel, the frequency ratio of the x-ray photons and the laser light, $\varkappa = \omega_X/\omega_L$, is Lorentz invariant, although each of the frequencies has to be Lorentz transformed individually when changing the frame of reference. The laser strength a_0 is Lorentz invariant as well [64]. That means no qualitatively different results are to be expected for the scattering off high-energy electrons. In addition, the energy transfer ℓ is a Lorentz invariant quantity and allows to characterise the frequency of the emitted photons in a Lorentz-invariant way via equation (5).

Let us finally discuss the case that the spectral resolution of our detector is too coarse to observe the individual caustic peaks. In figure 5 we show the spectra of the scattered x-rays for a detector resolution of 100 eV. Although the individual caustic peaks cannot be resolved due to the coarse detector resolution, the shape of the plateau strongly depends on the shape of the laser pulse. For the smooth $\cos^2$ laser pulse (solid blue curve and left inset) the caustic peaks are distributed over the whole plateau (dotted blue curve) and the coarse-grained spectrum shows a single peak close to the laser-free Compton line at about 5 keV, with falling shoulders up to the cut-off values at about 4 keV and 6.3 keV, respectively. In contrast to that, in the box-shaped pulse with a constant amplitude of the assisting laser, the caustic peaks occur only at the end-points of the plateau. Consequently, the coarse-grained spectrum has two peaks close to the cut-offs of the plateau. This shows that even if the details of the spectral caustic peaks are not resolved, their presence still influences the shape of the spectrum.

5. Summary and conclusions

In summary, we study for the first time the details of the frequency spectrum of x-rays that are Compton scattered off an electron under the action of an intense *ultra-short* optical laser pulse. In this laser-assisted Compton scattering of x-ray photons the frequency spectrum of the scattered x-rays shows novel features: a structured broad plateau region beneath the laser-free Compton line that indicates a highly nonlinear mixing of laser and x-ray photons. According to the QED calculation, the plateau region contains a number of sharp peaks that are related to the ultra-short duration of the assisting laser pulse. These peaks are explained by means of a semiclassical picture as spectral caustics with universal properties.

The laser-assisted Compton scattering of x-rays, and the peaks in the frequency spectrum, may be used to investigate the dynamics of laser-driven electrons in more general situations, where the electrons are also subject to forces other than the laser field. The three-dimensional electron motion could be accessed by observing tomographically the frequency spectrum of Compton scattered x-rays for different scattering directions n'. For instance, this might be useful to investigate the complex laser-driven electron dynamics at the surface of a dense

plasma, and could help to better understand the collisionless absorption of laser energy [65, 66], and its implications for plasma-based particle acceleration [67].

We finally note that the spectral caustics are a general concept. They could help understand also the dynamics of other laser-assisted scattering processes in ultra-short laser pulses [21, 23, 68]. For short laser pulses the spectral caustic peaks inevitably appear in the plateau regions of the spectra, and a proper description of the scattering dynamics with respect to the short laser pulse duration is mandatory. This is even true if the experimental conditions do not allow the direct observation of the individual caustic peaks, because their distribution over the plateau strongly affects the shape of the coarse-grained frequency spectra.

Acknowledgments

The authors gratefully acknowledge the stimulating discussions with T E Cowan, R Sauerbrey and Th Stöhlker within the HIBEF project.

Appendix A. Derivation of the differential cross section

The strong-field S matrix for laser-assisted Compton scattering of an x-ray photon from a short coherent XFEL pulse can be acquired by first formulating the Furry picture of strong field QED with respect to both the (weak) XFEL and (strong) assisting laser pulses. The resulting expressions are then linearised in the normalised amplitude of the XFEL pulse $a_{\rm X} \ll 1$ [69, 70]. The S matrix can be represented as [34]

$$S = -4\mathrm{i}e\pi^3\, a_{\rm X}\, \delta^{(3)}_{\rm l.f.}(p - p' - k')\boldsymbol{\mathcal{M}}(\ell), \tag{A.1}$$

with the light-front delta function

$$\delta^{(3)}_{\rm l.f.}(p - p' - k') \equiv \frac{1}{\omega_{\rm L}}\delta(p^- - p'^- - k'^-)\,\delta^{(2)}(\boldsymbol{p}_\perp - \boldsymbol{p}'_\perp - \boldsymbol{k}'_\perp) \tag{A.2}$$

and the light-front components of four-vectors $p^\pm = p^0 \pm p^3$ and $\boldsymbol{p}_\perp = (p^1, p^2)$. Here, p (p') refers to the asymptotic four-momentum of the electron before (after) the scattering, while k' is the four-momentum of the scattered x-ray photon. Due to the delta function in equation (A.1), the '$-$' and '$\perp$' momentum components fulfil conservation conditions, which can be written as

$$n\cdot p = n\cdot p' + n\cdot k' \qquad \text{and} \qquad \varepsilon_{\rm X,L}\cdot p = \varepsilon_{\rm X,L}\cdot p' + \varepsilon_{\rm X,L}\cdot k'. \tag{A.3}$$

The scattering amplitude

$$\boldsymbol{\mathcal{M}}(\ell; r, r', \lambda') = V_3(r, r', \lambda')C_0(\ell) - \alpha_{\rm X}\sum_{n=0}^{2} V_n(r, r', \lambda')C_n(\ell), \tag{A.4}$$

depends on the electron spin (r, r') and photon polarisation (λ') variables via the Dirac currents $V^j_n(r, r', \lambda') = \varepsilon'^{\mu}_{\lambda'}\,\bar{u}_{p'r'}(\mathcal{V}_n)_\mu u_{pr}$, where u_{pr} denote Dirac spinors, with the Dirac adjoint $\bar{u}_{pr} = u^\dagger_{pr}\gamma^0$, and normalised to $\bar{u}_{pr}u_{pr'} = 2m\delta_{rr'}$. The Dirac matrix structures read

$$(\mathcal{V}_0)_\mu = \gamma_\mu, \tag{A.5}$$

$$(\mathcal{V}_1)_\mu = m\left(\frac{\not{\varepsilon}_{\rm L}\not{k}_{\rm L}\gamma_\mu}{2k_{\rm L}\cdot p'} + \frac{\gamma_\mu\not{k}_{\rm L}\not{\varepsilon}_{\rm L}}{2k_{\rm L}\cdot p}\right), \tag{A.6}$$

$$(\mathcal{V}_2)_\mu = \frac{m^2\,\not{k}_{\rm L}\,k_{L,\mu}}{2p\cdot k_{\rm L}p'\cdot k_{\rm L}}, \tag{A.7}$$

$$(\mathcal{V}_3)_\mu = m\left(\frac{\not{\varepsilon}_{\rm X}\not{k}_{\rm X}\gamma_\mu}{2k_{\rm X}\cdot p'} + \frac{\gamma_\mu\not{k}_{\rm X}\not{\varepsilon}_{\rm X}}{2k_{\rm X}\cdot p}\right). \tag{A.8}$$

Here we employ the Feynman slash notation $\not{p} = \gamma\cdot p$ to denote scalar products of four-vectors with the Dirac matrices γ^μ. The dynamic integrals over the laser phase read

$$C_n(\ell) = \int \mathrm{d}\phi\; g_{\rm X}(\phi)\, a^n_{\rm L}(\phi)\, \mathrm{e}^{\mathrm{i}\int_{-\infty}^{\phi}\mathrm{d}\phi'\psi(\phi',\ell)}, \tag{A.9}$$

with $\psi(\phi, \ell)$ defined in equation (4). To calculate the differential cross section we have to square the S matrix (A.1), multiply by the Lorentz invariant phase space of the final particles in the form

$$\mathrm{d}\Pi = \frac{\mathrm{d}^3\,\mathrm{k}'}{(2\pi)^3\,2\omega'}\,\frac{\mathrm{d}p'^{-}\mathrm{d}^2\boldsymbol{p}'_{\perp}}{(2\pi)^3\,2p'^{-}}, \tag{A.10}$$

multiply with a normalisation factor of $1/2p^-$ for the incident Volkov electron state [71], and divide by the fluence of the incident x-rays

$$J_\mathrm{X} = \frac{1}{\omega_\mathrm{X}}\int_{-\infty}^{\infty}\mathrm{d}\phi\; T^{0i}_\mathrm{X}\, n_i = \frac{m^2\,a_\mathrm{X}^2}{8\pi\alpha}\int_{-\infty}^{\infty}\mathrm{d}\phi\; g_\mathrm{X}^2(\phi), \tag{A.11}$$

with the energy–momentum-tensor $T^{\mu\nu}_\mathrm{X}$ of the incident x-ray pulse. Then, the differential cross section for laser-assisted Compton scattering reads

$$\mathrm{d}\sigma(r',\,r,\,\lambda') = \frac{|S|^2}{2p^-J_\mathrm{X}}\mathrm{d}\Pi \tag{A.12}$$

$$= \frac{\alpha^2\omega'}{8\pi m^2\int_{-\infty}^{\infty}\mathrm{d}\phi\; g_\mathrm{X}^2(\phi)}\,\frac{|\mathcal{M}(\ell,\,r,\,r',\,\lambda')|^2}{k_\mathrm{L}\cdot p\;k_\mathrm{L}\cdot p'}\,\mathrm{d}\omega'\mathrm{d}\Omega, \tag{A.13}$$

and smoothly approaches the laser-free Klein–Nishina cross section in the limit $a_0 \to 0$ [34, 72]. Note that the cross section (A.13) is independent of the intensity of the XFEL beam and all dependence on a_X drops out.

Since we assume that the incident electrons are unpolarised, and we consider the polarisation of the final state particles unobserved, we have to average and sum over the respective variables, defining the polarisation averaged squared matrix element as

$$\langle|\mathcal{M}|^2\rangle = \frac{1}{2}\sum_{r,r',\lambda'}|\mathcal{M}(\ell;\,r,\,r',\,\lambda')|^2. \tag{A.14}$$

The summation over the spin variables leads to traces over the Dirac matrices that occur in the coefficients in equations (A.5)–(A.8). We define the Dirac traces as

$$\mathcal{T}_{nn'} \equiv \frac{1}{2}\sum_{r,r',\lambda'} V_n\,(V_{n'})^* = -\frac{1}{2}\mathrm{tr}[(\not{p}' + m)(\mathcal{V}_n)^\mu(\not{p} + m)(\bar{\mathcal{V}}_{n'})_\mu], \tag{A.15}$$

where we employ the identities $\sum_{\lambda'}(\varepsilon^\mu_{\lambda'})^*\varepsilon^\nu_{\lambda'} = -g^{\mu\nu}$, $\sum_r u_{pr}\bar{u}_{pr} = \not{p} + m$, and $\bar{\mathcal{V}} = \gamma^0\mathcal{V}^\dagger\gamma^0$. The Dirac traces read (note the symmetry $\mathcal{T}_{nn'} = \mathcal{T}_{n'n}$)

$$\mathcal{T}_{00} = -8m^2 + 4p'\cdot p, \tag{A.16}$$

$$\mathcal{T}_{10} = 2\,(k_\mathrm{L}\cdot k')\;\alpha_\mathrm{L}, \tag{A.17}$$

$$\mathcal{T}_{30} = 2\,(k_\mathrm{X}\cdot k')\;\alpha_\mathrm{X}, \tag{A.18}$$

$$\mathcal{T}_{20} = -2m^2, \tag{A.19}$$

$$\mathcal{T}_{11} = \mathcal{T}_{33} = 2\,m^2\eta \tag{A.20}$$

and all other combinations vanish. We use here the definitions from equation (2), and in addition

$$\alpha_\mathrm{L} = m\left(\frac{\varepsilon_\mathrm{L}\cdot p'}{k_\mathrm{L}\cdot p'} - \frac{\varepsilon_\mathrm{L}\cdot p}{k_\mathrm{L}\cdot p}\right). \tag{A.21}$$

Collecting all the non-vanishing Dirac traces, and using the identity

$$\ell C_0(\ell) = -\alpha_\mathrm{L}C_1(\ell) + \frac{m^2x}{2\,k_\mathrm{L}\cdot p}C_2(\ell) \tag{A.22}$$

we finally arrive at the expressions (1) and (2) for the polarisation averaged cross section and squared amplitude, respectively.

Appendix B. Efficient calculation of frequency averaged spectra

In this appendix we describe a method to efficiently calculate the window-averaged frequency spectra as exhibited, e.g., in figures 2 and 4. The integration of the squared matrix element (2) is numerically quite demanding because the integrand is a highly oscillating function of the laser phase. Moreover, because the frequency spectra are highly oscillating functions of the scattered photon energy one needs to calculate the spectra with a high precision to obtain a reliable frequency average. For the frequency-averaged spectra the highly oscillatory structure itself is irrelevant. The approximation presented here reduces the numerical cost in two ways: (i) one needs to calculate the spectrum at fewer points and (ii) the calculation of each point is accelerated.

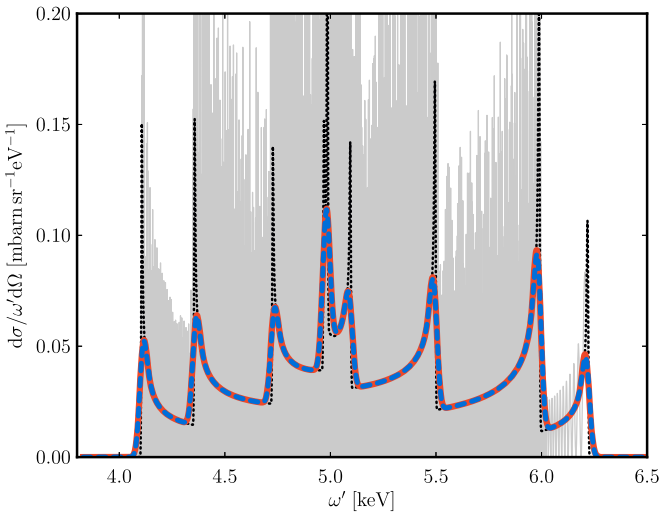

Figure B1. A direct comparison of the smoothed full spectrum (red solid curve) and the approximation (blue dashed curve) shows excellent agreement, i.e. the dashed blue curve is on top of the solid red curve. For the full spectrum the squared matrix element has been evaluated using equation (2), while we use equation (B.3) with $\Delta = 0.5$ for the approximated spectrum. Both of the spectra are then frequency averaged with the same window size of 15 eV. For comparison we also show the approximation (B.3) without the additional frequency average (black dotted curve), as well as the unsmoothed highly oscillating full spectrum (solid grey). Parameters are: $a_0 = 0.3$, $T_\mathrm{L} = 10$ fs, $T_\mathrm{X} = 15$ fs, $\cos^2$ pulse envelopes, $\vartheta = 45°$, $\varphi = 0$.

As we found in our semiclassical analysis, the highly oscillatory behaviour of the spectrum stems from the interference of distant stationary points. In order to suppress these spectral oscillations, we can include a (Gaussian) window function

$$w_\Delta(\phi - \phi') = \mathrm{e}^{-\frac{(\phi-\phi')^2}{4\Delta^2}} \tag{B.1}$$

to the integrand of equation (2), which suppresses the interference contributions for all phase points that are further apart than the window size Δ. The inverse of Δ is related to a frequency averaging window: the shorter the window size Δ, the coarser the energy resolution.

By introducing the relative and mean phase variables, $\theta = \phi - \phi'$ and $\tau = (\phi + \phi')/2$, and by requiring a small window size, $\Delta \ll 1$, we may assume that $\theta \ll 1$, to obtain for the short-time windowed squared matrix element:

$$\begin{aligned}\overline{\langle|\boldsymbol{\mathcal{M}}|^2\rangle} &= 2\,m^2 \int \mathrm{d}\tau\mathrm{d}\theta\; g_\mathrm{X}^2(\tau) w_\Delta(\theta)\; \mathrm{e}^{\mathrm{i}\int_{\tau-\theta/2}^{\tau+\theta/2}\mathrm{d}\phi\;\psi(\phi,\ell)}\left(\eta - 2\alpha_\mathrm{X}^2 - \frac{\alpha_\mathrm{X}^2\,\eta}{2}\,\theta^2\,\dot{a}_\mathrm{L}^2(\tau)\right)\\ &= (2\,m^2\eta - 4\,m^2\alpha_\mathrm{X}^2)\int \mathrm{d}\tau\; g_\mathrm{X}^2(\tau)\int \mathrm{d}\theta\; \mathrm{e}^{-\frac{\theta^2}{4\Delta^2}}\,\mathrm{e}^{\mathrm{i}\theta\psi(\tau,\ell)},\end{aligned} \tag{B.2}$$

where the third term in parentheses in the first line is of higher order in Δ and can be neglected. Evaluating the Gaussian integral over $\mathrm{d}\theta$ we finally find the simple expression

$$\overline{\langle|\boldsymbol{\mathcal{M}}|^2\rangle} = (2\,m^2\eta - 4\,m^2\alpha_\mathrm{X}^2)\sqrt{4\pi\Delta^2}\int \mathrm{d}\tau\; g_\mathrm{X}^2(\tau)\mathrm{e}^{-\Delta^2\psi^2(\tau,\ell)}, \tag{B.3}$$

which can be efficiently evaluated numerically. In particular, the exponent is now real and negative, i.e. the integrand is not a highly oscillating function anymore. In figure B1 we compare the frequency averaged spectra calculated using the exact squared matrix element (2) with the approximation equation (B.3). As can be inferred from figure B1 the accuracy of the approximation is excellent.

Taking in equation (B.3) the formal limit $\Delta \to \infty$ we get

$$\begin{aligned}\overline{\langle|\boldsymbol{\mathcal{M}}|^2\rangle}^{\Delta\to\infty} &= (2\,m^2\eta - 4\,m^2\alpha_\mathrm{X}^2)\;2\pi\int \mathrm{d}\tau\; g_\mathrm{X}^2(\tau)\delta(\psi(\tau,\,\ell))\\ &= (2\,m^2\eta - 4\,m^2\alpha_\mathrm{X}^2)\sum_j \frac{2\pi g_\mathrm{X}^2(\tau_j)}{|\dot{\psi}(\tau_j,\,\ell)|},\end{aligned} \tag{B.4}$$

where the sum runs over all stationary points $\psi(\tau_j, \ell) = 0$. This coincides with the usual stationary phase approximation of (2) with the interferences between different stationary points $j \neq j'$ excluded.

References

[1] Wernet P et al 2015 Nature 520 78
[2] Minitti M P et al 2015 Phys. Rev. Lett. 114 255501
[3] Kodama R et al 2001 Nature 412 798
[4] Marklund M and Shukla P K 2006 Rev. Mod. Phys. 78 591
[5] Glenzer S H and Redmer R 2009 Rev. Mod. Phys. 81 1625
[6] Fäustlin R et al 2010 Phys. Rev. Lett. 104 125002
[7] Kluge T, Gutt C, Huang L G, Metzkes J, Schramm U, Bussmann M and Cowan T E 2014 Phys. Plasmas 21 033110
[8] Hatchett S P et al 2000 Phys. Plasmas 7 2076
[9] Schwoerer H, Pfotenhauer S, Jäckel O, Amthor K U, Liesfeld B, Ziegler W, Sauerbrey R, Ledingham K W D and Esirkepov T 2006 Nature 439 445
[10] Metzkes J, Kluge T, Zeil K, Bussmann M, Kraft S D, Cowan T E and Schramm U 2014 New J. Phys. 16 023008
[11] Yanovsky V et al 2008 Opt. Express 16 2109
[12] Sarachik E S and Schappert G T 1970 Phys. Rev. D 1 2738
[13] Ritus V I 1985 J. Sov. Laser Res. 6 497
[14] Ehlotzky F, Krajewska K and Kamiński J Z 2009 Rep. Prog. Phys. 72 046401
[15] Di Piazza A, Müller C, Hatsagortsyan K Z and Keitel C H 2012 Rev. Mod. Phys. 84 1177
[16] Oleĭnik V P 1967 Sov. Phys. J. Exp. Theor. Phys. 25 697 (http://jetp.ac.ru/cgi-bin/e/index/e/25/4/p697?a=list)
[17] Lötstedt E, Jentschura U D and Keitel C H 2007 Phys. Rev. Lett. 98 043002
[18] Lötstedt E, Jentschura U D and Keitel C H 2008 Phys. Rev. Lett. 101 203001
[19] Voitkiv A B, Grün N and Ullrich J 2003 J. Phys. B: At. Mol. Opt. Phys. 36 1907
[20] Müller C, Voitkiv A B and Najjari B 2009 J. Phys. B: At. Mol. Opt. Phys. 42 221001
[21] Schnez S, Lötstedt E, Jentschura U D and Keitel C H 2007 Phys. Rev. A 75 053412
[22] Krajewska K 2011 Laser Phys. 21 1275
[23] Dadi A and Müller C 2012 Phys. Rev. C 85 064604
[24] Szymanowski C, Véniard V, Taïeb R and Maquet A 1997 Phys. Rev. A 56 3846
[25] Li S M, Berakdar J, Chen J and Zhou Z F 2004 J. Phys. B: At. Mol. Opt. Phys. 37 653
[26] Meuren S, Hatsagortsyan K Z, Keitel C H and Di Piazza A 2015 Phys. Rev. Lett. 114 143201
[27] Müller S J, Keitel C H and Müller C 2014 Phys. Rev. D 90 094008
[28] Ngoko Djiokap J M, Tetchou Nganso H M and Kwato Njock M G 2007 Phys. Scr. 75 726
[29] Kanya R, Morimoto Y and Yamanouchi K 2010 Phys. Rev. Lett. 105 123202
[30] Boca M 2013 Cent. Eur. J. Phys. 11 1123
[31] Roshchupkin S P 1996 Laser Phys. 6 837–58
[32] Roshchupkin S P, Lebed' A A, Padusenko E A and Voroshilo A I 2012 Laser Phys. 22 1113–4
Voroshilo A I, Roshchupkin S P and Nedoreshta V N 2015 J. Phys. B: At. Mol. Opt. Phys. 48 055401
Nedoreshta V N, Roshchupkin S P and Voroshilo A I 2015 Phys. Rev. A 91 062110
[33] Compton A H 1923 Phys. Rev. 21 483
[34] Seipt D and Kämpfer B 2014 Phys. Rev. A 89 023433
[35] Oleĭnik V P 1968 Sov. Phys. J. Exp. Theor. Phys. 26 1132 (http://jetp.ac.ru/cgi-bin/e/index/e/26/6/p1132?a=list)
[36] Guccione-Gush R and Gush H P 1975 Phys. Rev. D 12 404
[37] Akhiezer A I and Merenkov N P 1985 Sov. Phys. J. Exp. Theor. Phys. 61 41 (http://jetp.ac.ru/cgi-bin/e/index/e/61/1/p41?a=list)
Akhiezer A I and Merenkov N P 1985 Zh. Eksp. Teor. Fiz. 88 72
[38] Ehlotzky F 1989 J. Phys. B: At. Mol. Opt. Phys. 22 601
[39] Nedoreshta V N, Voroshilo A I and Roshchupkin S P 2013 Phys. Rev. A 88 052109
[40] Tavella F, Stojanovic N, Geloni G and Gensch M 2011 Nat. Photonics 5 162
[41] Hartmann N et al 2014 Nat. Photonics 8 706
[42] Schulz S et al 2015 Nat. Commun. 6 5938
[43] Berry M V and Upstill C 1980 Catastrophe optics: morphologies of caustics and their diffraction patterns Progress in Optics vol 18 (Amsterdam: North-Holland) p 257
[44] Kravtsov Y A and Orolov Y I 1983 Sov. Phys.—Usp. 26 1083
[45] Raz O, Pedatzur O, Bruner B D and Dudovich N 2012 Nat. Photonics 6 170
[46] Volkov D M 1935 Z. Phys. 94 250
[47] Mitter H 1975 Acta Phys. Austriaca Suppl. 14 397–468
[48] Glover T E et al 2012 Nature 488 603
[49] Reiss H R 2014 Phys. Rev. A 89 022116
[50] Seipt D, Rykovanov S G, Surzhykov A and Fritzsche S 2015 Phys. Rev. A 91 033402
[51] Kamiński J Z and Ehlotzky F 2006 J. Mod. Opt. 53 7
[52] Mackenroth F and Di Piazza A 2013 Phys. Rev. Lett. 110 070402
[53] Cowan T E and (the HIBEF collaboration) 2013 Status of the proposed Helmholtz International Beamline for Extreme Fields (HIBEF) European XFEL APS Division of Plasma Physics Meeting 2013 abstract NP8.063
[54] Englert T J and Rinehart E A 1983 Phys. Rev. A 28 1539
[55] Kilbourne C A, Bandler S R, Brown A D, Chervenak J A, Figueroa-Feliciano E, Finkbeiner F M, Iyomoto N, Kelley R L, Porter F S and Smith S J 2007 Proc. SPIE 6686 668606
[56] Pies C et al 2012 J. Low Temp. Phys. 167 269
[57] Hartemann F V, Fuchs S N, Sage G P L, Luhmann N C Jr, Woodworth J G, Perry M D, Chen Y J and Kerman A K 1995 Phys. Rev. E 51 4833
[58] Salamin Y I and Faisal F H M 1997 Phys. Rev. A 55 3678
[59] Arutyunian F R and Tumanian V A 1963 Phys. Lett. 4 176
[60] Schoenlein R W, Leemans W P, Chin A H, Volfbeyn P, Glover T E, Balling P, Zolotorev M, Kim K J, Chattopadhyay S and Shank C V 1996 Science 274 236
[61] Chouffani K, Wells D, Harmon F and Lancaster G 2002 Nucl. Instrum. Methods Phys. Res. A 495 95
[62] Hartemann F V and Wu S S Q 2013 Phys. Rev. Lett. 111 044801

[63] Sarri G et al 2014 Phys. Rev. Lett. 113 224801
[64] Heinzl T and Ilderton A 2009 Opt. Commun. 282 1879
[65] Brunel F 1987 Phys. Rev. Lett. 59 52
[66] Mulser P, Weng S M and Liseykina T 2012 Phys. Plasmas 19 043301
[67] Veltcheva M, Borot A, Thaury C, Malvache A, Lefebvre E, Flacco A, Lopez-Martens R and Malka V 2012 Phys. Rev. Lett. 108 075004
[68] Nousch T, Seipt D, Kämpfer B and Titov A I 2015 Spectral caustics in laser assisted breit-wheeler process (arXiv:1509.01983)
[69] Herrmann J and Zhukovskii V C 1972 Ann. Phys. (Leipzig) 482 349
[70] Hu H and Müller C 2011 Phys. Rev. Lett. 107 090402
[71] Ilderton A and Torgrimsson G 2013 Phys. Rev. D 87 085040
[72] Klein O and Nishina Y 1929 Z. Phys. 52 853